Computer Assisted Mechanics and Engineering Sciences, **10**: 69–79, 2003.

Logarithmic strain measure in finite element modelling of anisotropic hyperelastic materials

Paweł Dłużewski, Grzegorz Jurczak and Horacio Antúnez
Institute of Fundamental Technological Research, Polish Academy of Sciences
Świętokrzyska 21, 00-049 Warsaw, Poland

(Received January 10, 2001)

A new finite element to analyze problems of *anisotropic* hyperelasticity is presented. The constitutive equations are derived by means of the energy method, which leads to the stress measure conjugate to the logarithmic strain. Equilibrium equation are integrated in the current configuration. Multiplicative – instead of additive – decomposition of the time derivative of a strain tensor function is applied as a crucial step that makes possible the formulation for anisotropic hyperelastic materials. Unlike previous known anisotropic large deformation models, the one here presented assures the energy conservation while using the anisotropic elastic constants and the logarithmic strain measure. It is underlined that for the first time a model including all these features is presented. Some numerical examples are shown to illustrate the results obtained with this model and to compare them with other known anisotropic models.

Keywords: finite element method, logarithmic strain measure, elastic material, anisotropic material, constitutive behaviour

1. Introduction

The advanced analytical and numerical problems that arise throughout the modelling of thermodynamically accepted *anisotropic* elastic materials, is most surely the reason why the number of the anisotropic so-called hyperelastic finite elements available in commercial FE codes is very scarce, cf. ABAQUS, MARC, FEAP. Usually, they are limited to the Saint-Venant–Kirchhoff model based on the Green strain and eventually to the Biot model based upon the use of the Biot strain. Instead, these commercial packages offer most frequently a rich library of thermodynamically accepted *isotropic* elastic finite elements, in which the stress-strain relation can be fitted even to an arbitrarily chosen monotonically increasing curve e.g. that obtained in the uniaxial stress or strain tests.

On the other hand, there is an increasing need for such anisotropic hyperelastic models. Many of the recently manufactured materials are conceived as to develop very large strains in the elastic range. Moreover, a significant number of them are anisotropic. Therefore the use of new finite elements that can better fit the anisotropic behaviour of real materials is very desired.

Most of the theoretical papers devoted to nonlinear elasticity fall mainly into two categories: (a) isotropic hyperelasticity and (b) isotropic and anisotropic hypoelasticity. It is worth emphasizing that *hypo*elastic materials, contrary to *hyper*elastic, ignore the potential character of energy. Therefore, hypoelastic finite elements often describe nothing but a perpetual motion producing or annihilating energy (work) in closed deformation loops — depending on the loop direction. Our interest is focused here, as said on the constitutive models based on the logarithmic strain measure, cf. [1, 4–8, 10, 15]. To ascertain whether a given constitutive model describes the hyperelastic (Green) or at least the Cauchy elastic material, additional theorems are studied in *hypo*elasticity, cf. [15]. Regarding *anisotropy*, the problem is more complicated and, therefore, considerations are often limited only to remarks stating that the stress conjugate to logarithmic strain is then not coaxial to the stretch tensor, what implies a complex relation between the Cauchy stress and the conjugate stress to logarithmic strain.

In this paper the model for an anisotropic hyperelastic material is implemented into a finite element code. In the next section the constitutive equations are derived from energy considerations. Two approaches based, respectively, upon the Lagrangian and Eulerian tensors are simultaneously developed. Two fourth order tensors characterize the thus arising relations. Next, the discretization into finite elements is briefly presented, and, finally, some numerical examples show the behaviour of the model and its comparison with the linear strain measure.

2. Logarithmic hyperelasticity

2.1. Introductory comments

In this section we shall derive the form the constitutive equations assume for an anisotropic hyperelastic material when logarithmic strain measure is used. It will result by considering the energy balance equation, which must be fulfilled for any arbitrarily chosen velocity gradient, as we will see later on. Keeping in mind the polar decomposition of the deformation gradient into the rotation $\mathbf{R}$, and the right or left stretch tensors, $\mathbf{U}$ and $\mathbf{V}$, respectively,

$$\mathbf{F} = \mathbf{VR} = \mathbf{RU} \tag{1}$$

we will arrive at expressions for the different quantities entering the model written in the current configuration based on either the left and right stretch tensors. In passing, the decomposition into eigenvalues and eigenvectors of the stretch tensors provides us a suitable basis to write a general expression of the strain measure of which the logarithmic strain is a particular case. On these bases we will obtain auxiliary tensors to complete the constitutive equations.

2.2. Logarithmic strain measure

Making use of the sets of eigenvalues u_i, v_i and eigenvectors $\mathbf{u}_i$, $\mathbf{v}_i$, (with $i = 1, \ldots, N$ and N = space dimension) of the right and left stretch tensors, respectively, we define the Lagrangian $\widehat{\boldsymbol{\varepsilon}}$ and Eulerian $\boldsymbol{\varepsilon}$ strain tensors as those which can be decomposed as

$$\widehat{\boldsymbol{\varepsilon}} \stackrel{\text{df}}{=} \sum_{I=1,3} f(u_I)\, \mathbf{u}_I \otimes \mathbf{u}_I \qquad \text{and} \qquad \boldsymbol{\varepsilon} \stackrel{\text{df}}{=} \sum_{i=1,3} f(v_i)\, \mathbf{v}_i \otimes \mathbf{v}_i, \tag{2}$$

where $f(\cdot)$ denotes an arbitrarily chosen C^1 monotonically increasing function $f(x) : R^+ \ni x \to f \in R$ which satisfies

$$f(x)|_{x=1} = 0, \tag{3}$$

$$\left.\frac{\mathrm{d}f(x)}{\mathrm{d}x}\right|_{x=1} = 1. \tag{4}$$

Conditions (3) and (4) assure compatibility with the Cauchy strain measure at small strains.

It can be shown that the decomposition given in Eq. (2) can be applied to the so-called generalized Lagrangian and Eulerian strain measures [4, 12]

$$\widehat{\boldsymbol{\varepsilon}} = \frac{1}{n}(\mathbf{U}^n - \mathbf{1}) \qquad \text{and} \qquad \boldsymbol{\varepsilon} = \frac{1}{n}(\mathbf{V}^n - \mathbf{1}), \tag{5}$$

with $n \neq 0$, while $n = 0$ yields the logarithmic strain tensors, which are defined as

$$\widehat{\boldsymbol{\varepsilon}} \stackrel{\text{df}}{=} \ln \mathbf{U} \qquad \text{and} \qquad \boldsymbol{\varepsilon} \stackrel{\text{df}}{=} \ln \mathbf{V}. \tag{6}$$

2.3. Constitutive equations

We now consider the energy balance, from which we will obtain the condition that yields the constitutive equation. For an isothermal and quasi-static deformation process within the elastic range we write

$$-\rho\dot{\psi} + \boldsymbol{\sigma} : \mathbf{d} = 0, \tag{7}$$

where ρ is the mass density, ψ the specific strain energy, $\boldsymbol{\sigma}$ the Cauchy stress tensor and $\mathbf{d}$ the symmetric part of the velocity gradient, which can be written e.g. as

$$\mathbf{d} = \frac{1}{2}\mathbf{R}(\dot{\mathbf{U}}\mathbf{U}^{-1} + \mathbf{U}^{-1}\dot{\mathbf{U}})\mathbf{R}^T = \frac{1}{2}(\nabla\mathbf{v} + \nabla^T\mathbf{v}) \tag{8}$$

where $\mathbf{v}$ denotes the velocity vector. In what follows we assume that the specific strain energy ψ can be written as a function of only the Lagrangian strain tensor, as required by the hyperelastic model

$$\psi = \psi(\widehat{\boldsymbol{\varepsilon}}). \tag{9}$$

Thus its time derivative as called for in Eq. (7) will read

$$\dot{\psi} = \frac{\partial\psi}{\partial\widehat{\boldsymbol{\varepsilon}}} : \dot{\widehat{\boldsymbol{\varepsilon}}}. \tag{10}$$

Using Eq. (2) it can be shown that

$$\dot{\widehat{\boldsymbol{\varepsilon}}} = \widehat{\boldsymbol{\mathcal{A}}} : (\mathbf{R}^T\,\mathbf{d}\,\mathbf{R}) \tag{11}$$

where $\widehat{\boldsymbol{\mathcal{A}}}$ is a fourth-order tensor. $\widehat{\boldsymbol{\mathcal{A}}}$ decomposed in the eigenvector basis $\mathbf{u}_i$ is represented by the following non-vanishing components [5]

$$\widehat{\mathcal{A}}_{IJIJ} = \begin{cases} \delta_{IJ} u_I f'(u_i) & \text{for } u_I = u_J, \\ \dfrac{u_I u_J [f(u_I) - f(u_J)]}{u_I{}^2 - u_J{}^2} & \text{for } u_I \neq u_J, \end{cases} \tag{12}$$

where $\widehat{\mathcal{A}}_{IJIJ} = \widehat{\mathcal{A}}_{IJJI} = \widehat{\mathcal{A}}_{JIIJ}$. Substituting Eqs. (10) and (11) into Eq. (7) we obtain

$$-\frac{\rho}{\widehat{\rho}}\left(\widehat{\rho}\frac{\partial\psi}{\partial\widehat{\boldsymbol{\varepsilon}}}\right) : \widehat{\boldsymbol{\mathcal{A}}} : (\mathbf{R}^T\,\mathbf{d}\,\mathbf{R}) + \boldsymbol{\sigma} : \mathbf{d} = 0, \tag{13}$$

where $\widehat{\rho} = \rho \det\mathbf{F}$.

By inspection of Eq. (13) we see that, since the energy balance must hold for any value of the symmetric part of the strain velocity $\mathbf{d}$, the following expression for the Cauchy stress tensor arises

$$\boldsymbol{\sigma} = \mathbf{R}\left(\widehat{\boldsymbol{\mathcal{A}}} : \widehat{\rho}\frac{\partial\psi}{\partial\widehat{\boldsymbol{\varepsilon}}}\right)\mathbf{R}^T \det\mathbf{F}^{-1} \tag{14}$$

which, by defining $\widehat{\boldsymbol{\sigma}}$ as the stress measure conjugate to the Lagrangian strain tensor $\widehat{\boldsymbol{\varepsilon}}$,

$$\widehat{\boldsymbol{\sigma}} \overset{\text{df}}{=} \widehat{\rho}\frac{\partial\psi}{\partial\widehat{\boldsymbol{\varepsilon}}}, \tag{15}$$

can be rewritten in the form of a transformation rule between $\boldsymbol{\sigma}$ and $\widehat{\boldsymbol{\sigma}}$

$$\boldsymbol{\sigma} = \mathbf{R}\,(\widehat{\boldsymbol{\mathcal{A}}} : \widehat{\boldsymbol{\sigma}})\,\mathbf{R}^T \det\mathbf{F}^{-1}. \tag{16}$$

A more detailed discussion of the constitutive model (15) is given by Dłużewski in [3]. For example, if we assume the specific strain energy function for a hyperelastic material in the form

$$\psi = \frac{1}{2\widehat{\rho}}\,\widehat{\boldsymbol{\varepsilon}} : \widehat{\mathbf{D}} : \widehat{\boldsymbol{\varepsilon}}, \tag{17}$$

where $\widehat{\mathbf{D}}$ is a fourth-order tensor of elastic stiffness, then we can calculate $\frac{\partial \psi}{\partial \widehat{\boldsymbol{\varepsilon}}}$ and substitute into Eq. (14) to get

$$\boldsymbol{\sigma} = \mathbf{R}\,(\widehat{\boldsymbol{\mathcal{A}}} : \widehat{\mathbf{D}} : \widehat{\boldsymbol{\varepsilon}})\,\mathbf{R}^T \det \mathbf{F}^{-1}, \tag{18}$$

which can be finally written in terms of tensorial measures referred to the current configuration as

$$\boldsymbol{\tau} = \boldsymbol{\mathcal{A}} : \mathbf{D} : \boldsymbol{\varepsilon}, \tag{19}$$

where $\boldsymbol{\tau}$ denotes the Kirchhoff stress, and

$$\boldsymbol{\tau} \stackrel{\text{df}}{=} \boldsymbol{\sigma} \det \mathbf{F}, \qquad D^{klmn} = R^k{}_K\, R^l{}_L\, R^m{}_M\, R^n{}_N\, \widehat{D}^{KLMN}, \tag{20}$$

$$\boldsymbol{\varepsilon} \stackrel{\text{df}}{=} \mathbf{R}\widehat{\boldsymbol{\varepsilon}}\mathbf{R}^T, \qquad \mathcal{A}^{klmn} = R^k{}_K\, R^l{}_L\, R^m{}_M\, R^n{}_N\, \widehat{\mathcal{A}}^{KLMN}. \tag{21}$$

Eqs. (18) and (19) give the constitutive stress-strain equations for an anisotropic hyperelastic material with the specific strain energy function given by Eq. (17). In correspondence to different choices of the strain measure, different expressions for the fourth-order tensors $\widehat{\boldsymbol{\mathcal{A}}}$ and $\boldsymbol{\mathcal{A}}$ will be obtained. For the logarithmic strain measure they read, after decomposition in the eigenvector bases

$$\widehat{\mathcal{A}}_{IJIJ} = \begin{cases} \delta_{IJ} & \text{for } \widehat{\varepsilon}_I = \widehat{\varepsilon}_J \\ \dfrac{\widehat{\varepsilon}_I - \widehat{\varepsilon}_J}{e^{\widehat{\varepsilon}_I - \widehat{\varepsilon}_J} - e^{\widehat{\varepsilon}_J - \widehat{\varepsilon}_I}} & \text{for } \widehat{\varepsilon}_I \neq \widehat{\varepsilon}_J \end{cases} \tag{22}$$

$$\mathcal{A}_{ijij} = \begin{cases} \delta_{ij} & \text{for } \varepsilon_i = \varepsilon_j \\ \dfrac{\varepsilon_i - \varepsilon_j}{e^{\varepsilon_i - \varepsilon_j} - e^{\varepsilon_j - \varepsilon_i}} & \text{for } \varepsilon_i \neq \varepsilon_j \end{cases} \tag{23}$$

while the remaining components vanish. This completes the model for the anisotropic hyperelastic material described with the logarithmic strain measure. We may notice that whenever the components of the tensors rewritten in eigenvector bases satisfy $\widehat{\varepsilon}_I = \varepsilon_i$, we find $\widehat{\mathcal{A}}_{IJIJ} = \mathcal{A}_{ijij}$, what does not mean that $\boldsymbol{\mathcal{A}} = \widehat{\boldsymbol{\mathcal{A}}}$ nor $\boldsymbol{\varepsilon} = \widehat{\boldsymbol{\varepsilon}}$, cf. Eq. (21b).

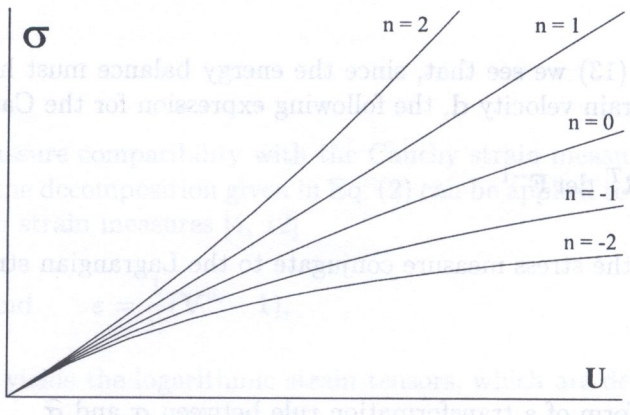

Fig. 1. Cauchy stress versus various strain measures applied in Eq. (18) for uniaxial stress

The above considerations are valid for any kind of hyperelastic materials, i.e. either isotropic and anisotropic. Specifically, concerning the use of the logarithmic strain measure, up to now the proposed models have been restricted mainly to the isotropic case [6, 9, 11] because anisotropy causes the stress conjugate to logarithmic strains to be not coaxial with the stretch tensor, resulting in a complex relation between the conjugate and the Cauchy stress. The larger the strains, the elastic behaviour of constitutive models based on the generalized strain tensor differs more from each other. Figure 1 shows the comparison of the behaviour of isotropic hyperelastic models based upon Eqs. (18) and (5) for various strain parameter n.

3. Finite element method

The physical model presented in the previous section has been implemented within the finite element method. As a result, a computational tool for analyzing non-standard problems, namely those involving large-strain deformation processes of anisotropic hyperelastic materials has been developed. The general discretization patterns used in the finite element method have been followed, but accounting for the specific features of the present problem.

We start considering the weighted equilibrium equation in its weak form, where, following the Galerkin method, the weighting functions are equal to the shape functions $\mathbf{N}$ in terms of which the displacement field is discretized ($\mathbf{u} = \mathbf{N}^T\mathbf{a}$)

$$\int_v N_i \sigma_{ij,j} \, \mathrm{d}v = \int_v N_i f_j \, \mathrm{d}v, \tag{24}$$

where v is the discretized domain in the current configuration, ∂v its boundary, and f volume distributed forces. By integrating by parts the left-hand side of Eq. (24) we can write

$$\int_v N_{i,j} \sigma_{ij} \, \mathrm{d}v = -\int_v N_i f_j \, \mathrm{d}v + \int_{\partial v} N_i \sigma_{ij} n_j \, \mathrm{d}(\partial v), \tag{25}$$

where n_j is the outward normal vector to the boundary ∂v. In the above system of equations it is the discretized displacement a_i that it is solved for. The actual configuration and the stress tensor (through the strain tensor and the proper transformation) are functions of them. Since Eq. (25) is non-linear in the discretized variables, it is solved by iterations. To this aim we write it in residual form as

$$\mathbf{P}(\mathbf{a}) = \int_v N_{i,j} \sigma_{ij} \, \mathrm{d}v + \int_v N_i f_j \, \mathrm{d}v - \int_{\partial v} N_i \sigma_{ij} n_j \, \mathrm{d}(\partial v). \tag{26}$$

To arrive at the solution of Eq. (26) we require

$$\|\mathbf{P}(\mathbf{a})\| < \delta, \tag{27}$$

where δ is a convergence tolerance. To meet this condition we calculate the correction to the solution vector $\mathbf{a}$ so as to zero a one term series expansion of the residual at $\mathbf{a}$. Denoting with a right upper index the iteration number, we require that

$$\mathbf{P}(\mathbf{a}^{\omega+1}) = \mathbf{P}(\mathbf{a}^{\omega}) + \frac{\partial \mathbf{P}(\mathbf{a}^{\omega})}{\partial \mathbf{a}} (\mathbf{a}^{\omega+1} - \mathbf{a}^{\omega}) = \mathbf{0} \tag{28}$$

from which we solve for $(\mathbf{a}^{\omega+1} - \mathbf{a}^{\omega})$ using the so-called tangent matrix as the system matrix

$$\begin{aligned}
\mathbf{K} = \frac{\partial \mathbf{P}}{\partial \mathbf{a}} &= \frac{\partial \int_v \nabla \mathbf{N} \, \boldsymbol{\sigma}(\mathbf{a}) \, \mathrm{d}v}{\partial \mathbf{a}} = \frac{\partial \int_V \nabla \mathbf{N} \, \boldsymbol{\sigma}(\mathbf{a}) \, \frac{\mathrm{d}v}{\mathrm{d}V} \, \mathrm{d}V}{\partial \mathbf{a}} = \int_V \frac{\partial [\nabla \mathbf{N} \, \boldsymbol{\sigma}(\mathbf{a}) \, \frac{\mathrm{d}v}{\mathrm{d}V}] \, \mathrm{d}V}{\partial \mathbf{a}} \\
&= \int_V \frac{\partial (\nabla \mathbf{N})}{\partial \mathbf{a}} \boldsymbol{\sigma}(a) \, \frac{\mathrm{d}v}{\mathrm{d}V} \, \mathrm{d}V + \int_V \nabla \mathbf{N} \, \frac{\partial [\boldsymbol{\sigma}(\mathbf{a}) \, \frac{\mathrm{d}v}{\mathrm{d}V}]}{\partial \mathbf{a}} \, \mathrm{d}V \\
&= \int_v \frac{\partial (\nabla \mathbf{N})}{\partial \mathbf{a}} \boldsymbol{\sigma}(a) \, \mathrm{d}v + \int_V \nabla \mathbf{N} \, \frac{\partial [\boldsymbol{\sigma}(\mathbf{a}) \frac{\mathrm{d}v}{\mathrm{d}V}]}{\partial \mathbf{a}} \, \frac{\mathrm{d}V}{\mathrm{d}v} \, \mathrm{d}v.
\end{aligned} \tag{29}$$

Due to the complex dependencies on $\mathbf{a}_i$ this derivative has been calculated numerically. An approximate tangent matrix has been also used by dropping the first term in Eq. (29), i.e.

$$\mathbf{K}_{ij} \approx \int_v \nabla \mathbf{N}_i \frac{\partial[\boldsymbol{\sigma}(\mathbf{a}) \det \mathbf{F}]}{\partial \mathbf{a}_j} \det \mathbf{F}^{-1} \, dv, \tag{30}$$

which does not affect the results since we are solving the same problem, defined by the residual $\mathbf{P}(\mathbf{a})$. Eventually, the rate of convergence may be affected but, according to our experience, it did not, at least in the examples we solved. The constitutive model has been implemented into the FEAP program [16] as a new user element. The problem was discretized with nine-node biquadratic elements.

4. Numerical examples

The model for anisotropic hyperelasticity with logarithmic strain measure has been used to solve a number of simple problems, some of which are presented in this Section. They have been designed so as to highlight the behaviour of the model under different deformation processes. The results have been compared with the St.Venant-Kirchhoff model and the linear model for small deformations. Since anisotropic models are not available, only qualitative behaviour is evaluated in this respect.

The examples presented below simulate the deformation in 2D of CdTe crystal specimens in elastic range. CdTe is a crystal with cubic symmetry and only three elastic constants describe its elastic properties (cf. [14]),

$$\begin{aligned} &D_{1111} = D_{11} = 53.5 \cdot 10^9 \text{ [Pa]}, \qquad D_{1212} = D_{12} = 36.8 \cdot 10^9 \text{ [Pa]}, \\ &D_{4444} = D_{44} = 19.9 \cdot 10^9 \text{ [Pa]}. \end{aligned} \tag{31}$$

Example 1

We first consider a rectangular specimen subject to a uniaxial stress state imposed by means a set of x-forces on one edge, while x-displacements on the other are constrained. Both induce a uniform loading throughout the element, as that of a constant distributed load. On the y-direction the constraints are only applied on the symmetry axis in order to avoid rigid body displacement modes, thus zero σ_y and τ_{xy} stresses are obtained. The scheme of the model is shown in Fig. 2, where also

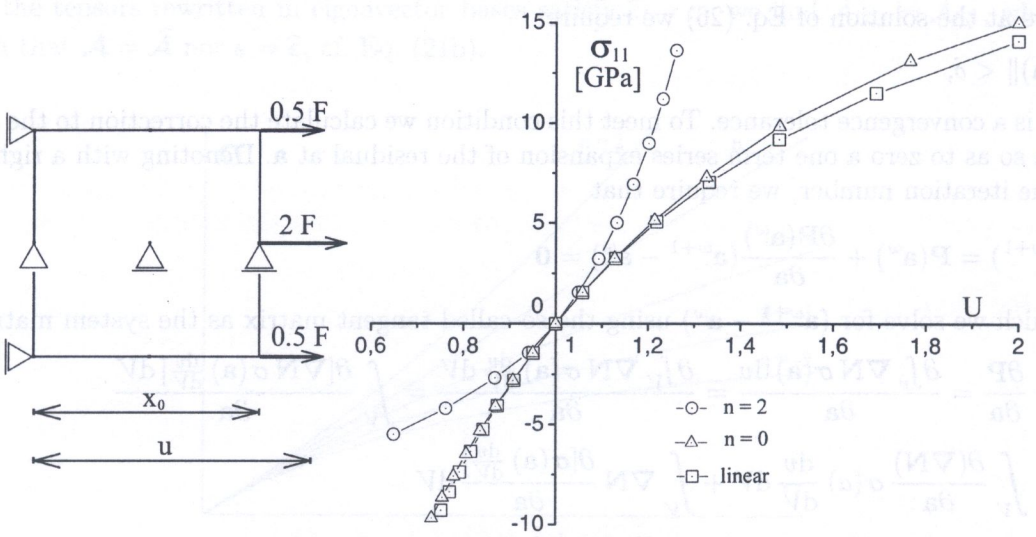

Fig. 2. Layout and response diagram for uniaxial stress

the stress-strain results have been plotted for the three models considered: logarithmic ($n = 0$), St.Venant–Kirchhoff ($n = 2$) and linear. The different behaviour of the two large strain models can be clearly noticed. The one based on the logarithmic strain measure is qualitatively closer to the linear model, while the St. Venant–Kirchhoff diverges very quickly with growing strains. Further insight is gained by considered the logarithmic strain. In our example the linear strain is calculated as

$$\varepsilon = \frac{u}{x_o} \tag{32}$$

while the logarithmic strain reads

$$\varepsilon_{ln} = \ln \frac{x_o + u}{x_o}. \tag{33}$$

The plot of the stress–logarithmic-strain curve, shown in Fig. 3, highlights the fact that the model based on the logarithmic strain measure remains along a linear stress-strain behaviour, while, for geometric reasons, the linear model softens. Both for traction and compression the St.Venant-Kirchhoff model hardens unrealistically.

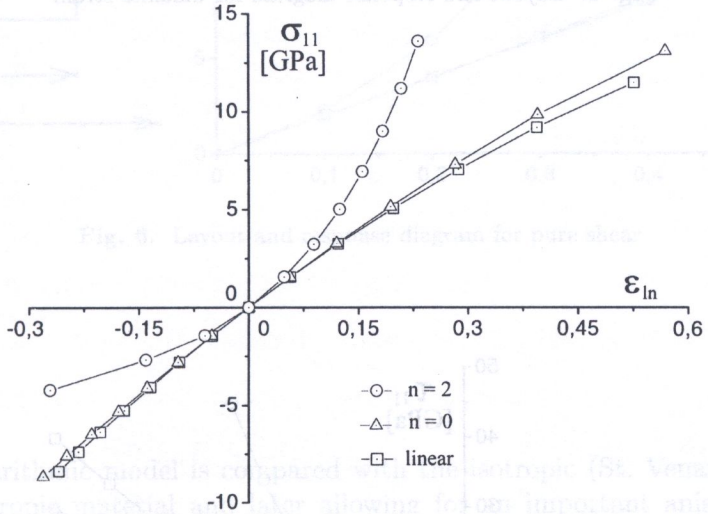

Fig. 3. Kirchhoff stress – logarithmic strain diagram for uniaxial stress

Example 2

In the second example the same element already considered is subject to the same loading but now under different displacement restrictions, namely all the y-displacements are constrained. Thus the obtained x-displacements will uniquely define the volume variation. The reaction forces on the y-direction will induce σ_x and σ_y stresses resulting in a hydrostatic stress added to the uniaxial stress. The same material as in the first example, with its elasticity constants is used.

The plot shown in Fig. 4 shows that the stress state strongly depends on the imposed boundary conditions. All the models exhibit a nonlinear behaviour. However, by plotting the Kirchhoff stress, cf. Eq. (19) *vs* the logarithmic strain, we obtain a linear stress-strain behaviour for the logarithmic model, while both the linear and St. Venant–Kirchhoff models are more stiff, see Fig. 5.

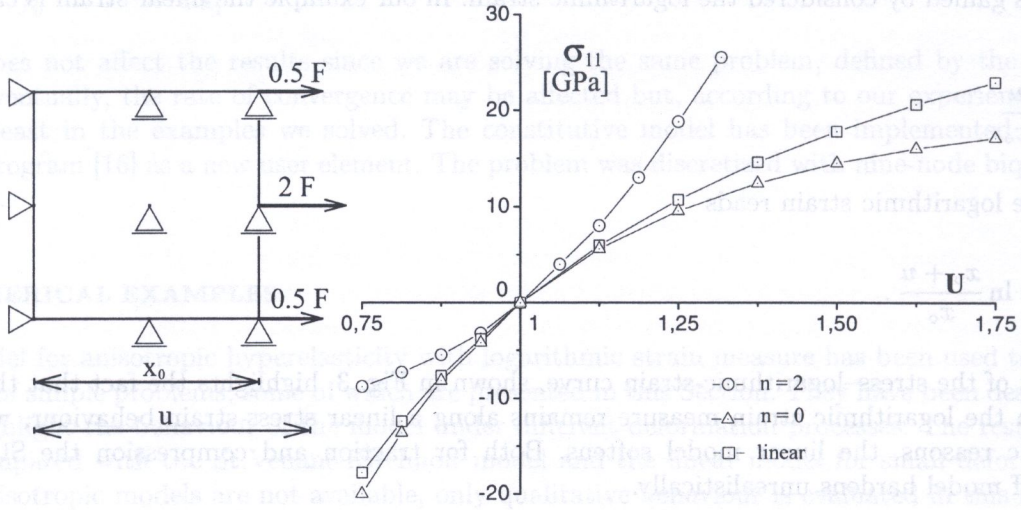

Fig. 4. Layout and response diagram for uniaxial strain

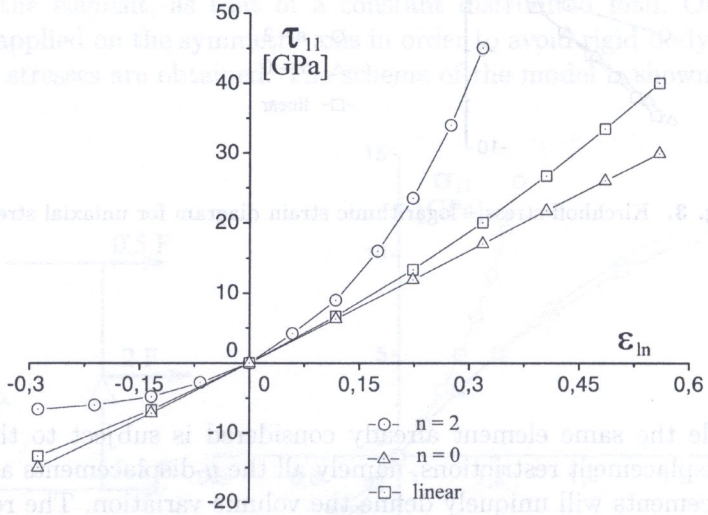

Fig. 5. Kirchhoff stress – logarithmic strain diagram for uniaxial strain

Example 3

The next example considers again our specimen of the same material properties as before, but now subject to pure shear. Boundary and load conditions have been accordingly modified. Displacements have been imposed as shown in Fig. 6. In the same figure the stresses calculated with the three models are plotted in terms of the logarithmic strain. Again we obtain the linear behaviour for the logarithmic model and a growing instantaneous stiffness for the other two models. Its easy to notice that the St. Venant–Kirchhoff model is significantly stiffer and under large strain inducing an adequately higher stress in comparison with other models examined in this example.

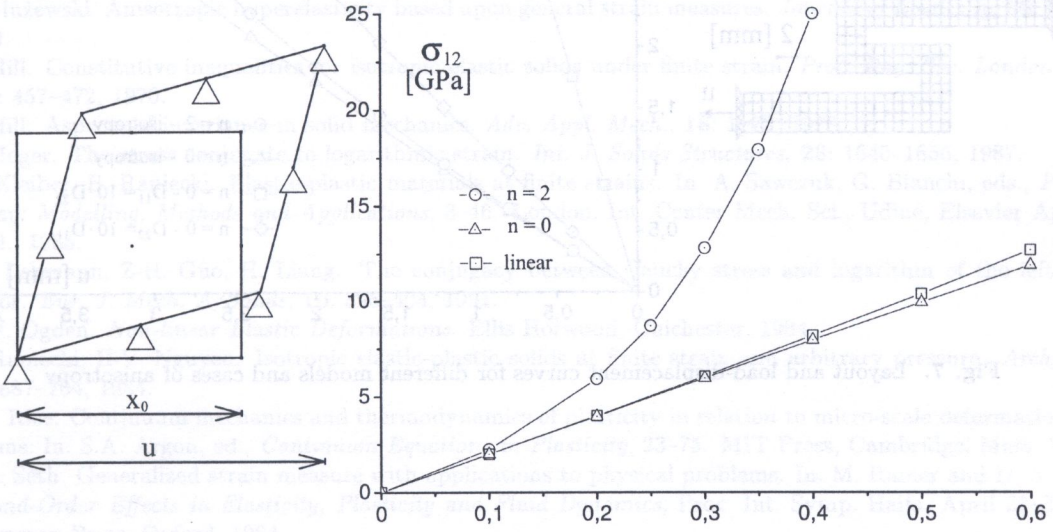

Fig. 6. Layout and response diagram for pure shear

Example 4

The anisotropic-logarithmic model is compared with the isotropic (St. Venant–Kirchhoff) one assuming first an isotropic material and later allowing for an important anisotropy in one of the material directions. The problem layout is schematized in Fig. 7. A uniform horizontal displacement field is applied to the right end of a 'z'-shaped specimen while the other end is fixed. Because of the geometry the displacement field involves both in-plane components.

First, an isotropic material is solved for using the logarithmic-strain based, and the St. Venant–Kirchhoff models. Afterwards, anisotropy is obtained by assuming different elastic constants, which in this problem will be equivalent to a horizontal and vertical reinforcement respectively. Both cases are solved within the anisotropic-logarithmic model. The resulting final configurations are shown in Fig. 8.

The final shapes and the respective load-displacement curves (cf. Fig. 7) show that similar results are obtained with logarithmic and St. Venant–Kirchhoff models for the isotropic case. For the anisotropic material we obtain a stiffer behaviour especially for the case of reinforcement in the direction of imposed displacements. For the isotropic case, we can see that the most noticeable differences between logarithmic and St. Venant–Kirchhoff models appear in the regions where displacements are relatively large. In this problem, the dominant strain mode is that of bending, where the stress distribution will be that of σ_x . Thus, if the corresponding elastic constant has been enlarged, we can expect a more stiff behaviour of this element, as it happens.

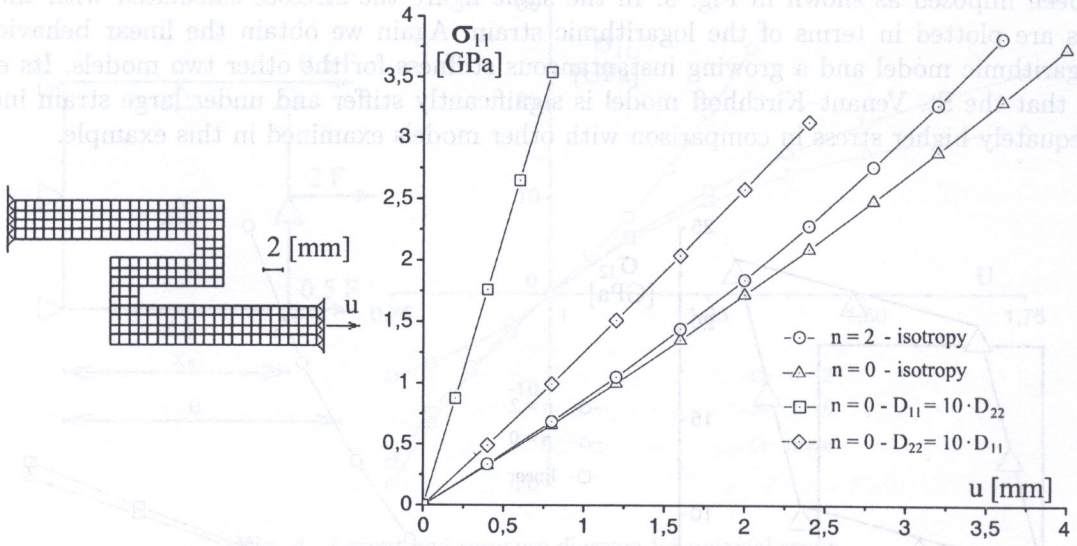

Fig. 7. Layout and load-displacement curves for different models and cases of anisotropy

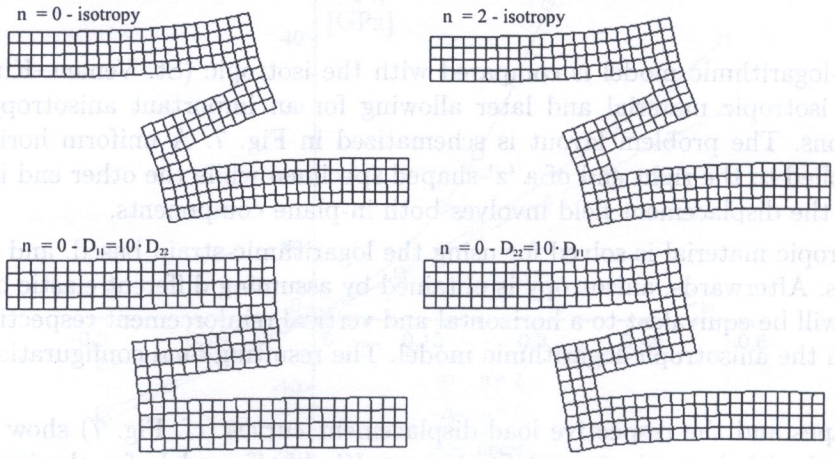

Fig. 8. Final shapes for different cases of anisotropy

ACKNOWLEDGMENT

This research was supported by the State Committee for Scientific Research (KBN) in Poland under Grant No. 7 T07A 015 17.

REFERENCES

[1] L. Anand. On H. Hencky approximate strain-energy function for moderate deformations. *Transactions of ASME*, **46**: 78–82, 1979.

[2] M.A. Crisfield. *Nonlinear Finite Element Analysis of Solids and Structures*, Vol. II – *Advanced Topics*. Wiley, Chichester, 1997.

[3] P. Dłużewski. Anisotropic hyperelasticity based upon general strain measures. *Journal of Elasticity*, **60**: 119–129, 2000.

[4] R. Hill. Constitutive inequalities for isotropic elastic solids under finite strain. *Proc. Roy. Soc. London Ser. A*, **314**: 457–472, 1970.

[5] R. Hill. Aspects of invariance in solid mechanics. *Adv. Appl. Mech.*, **18**: 1–75, 1978.

[6] A. Hoger. The stress conjugate to logarithmic strain. *Int. J. Solids Structures*, **23**: 1645–1656, 1987.

[7] M. Kleiber, B. Raniecki. Elastic-plastic materials at finite strains. In: A. Sawczuk, G. Bianchi, eds., *Plasticity Today: Modelling, Methods and Applications*, 3–46. London, Int. Center Mech. Sci., Udine, Elsevier Appl. Sci. Publ., 1985.

[8] Th. Lehmann, Z-H. Guo, H. Liang. The conjugacy between Cauchy stress and logarithm of the left stretch tensor. *Eur. J. Mech. A/Solids*, **10**: 395–404, 1991.

[9] R.W. Ogden. *Non-linear Elastic Deformations*. Ellis Horwood, Chichester, 1984.

[10] B. Raniecki, H.V. Nguyen. Isotropic elastic-plastic solids at finite strain and arbitrary pressure. *Arch. Mech.*, **36**: 687–704, 1984.

[11] J.R. Rice. Continuum mechanics and thermodynamics of plasticity in relation to micro-scale deformation mechanisms. In: S.A. Argon, ed., *Continuum Equations in Plasticity*, 23–75. MIT Press, Cambridge, Mass, 1975.

[12] B.R. Seth. Generalized strain measure with applications to physical problems. In: M. Rainer and D. Abir, eds., *Second-Order Effects in Elasticity, Plasticity and Fluid Dynamics*, Proc. Int. Symp. Haifa, April 23–27, 1962. Pergamon Press, Oxford, 1964.

[13] S.V. Vaidya, G.C. Kennedy. Compressibility of 22 elemental solids to 45KB. *J. Phys. Chem. Solids.*, **31**: 2329–2345, 1970.

[14] N. J. Walker, G.A. Saunders, J.E. Hawkey. Soft TA models and anharmonicity in cadmium telluride. *Physical Review B*, **52**(5): 1005–1018, 1985.

[15] H. Xiao, O.T. Bruhns, A. Meyers. Hypo-elasticity model based upon the logarithmic stress rate. *J. Elasticity*, **47**: 51–68, 1997.

[16] O.C. Zienkiewicz, R.J. Taylor. *The Finite Element Method*. McGraw-Hill, London, 1991.